COMPLIS experiments: COllaboration for spectroscopy Measurements using a Pulsed Laser Ion Source

J. Sauvage [a], N. Boos [b,*], L. Cabaret [c], J.E. Crawford [d], H.T. Duong [c], J. Genevey [e], M. Girod [f], G. Huber [b], F. Ibrahim [a,e], M. Krieg [b], F. Le Blanc [a], J.K.P. Lee [d], J. Libert [g], D. Lunney [a,i], J. Obert [a], J. Oms [a], S. Péru [f], J. Pinard [c], J.C. Putaux [a], B. Roussière [a], V. Sebastian [b], D. Verney [a], S. Zemlyanoi [a,**], J. Arianer [a], N. Barré [a], M. Ducourtieux [a], D. Forkel-Wirth [h], G. Le Scornet [h,i], J. Lettry [h], C. Richard-Serre [h,j], C. Véron [a] and the ISOLDE Collaboration

[a] *Institut de Physique Nucléaire, IN2P3-CNRS, F-91406 Orsay Cedex, France*
[b] *Institut für Physik der Universität Mainz, D-55099 Mainz, Germany*
[c] *Laboratoire Aimé Cotton, F-91405 Orsay Cedex, France*
[d] *Physics Department, McGill University, Montréal, Canada H3A 2T8*
[e] *Institut des Sciences Nucléaires, IN2P3-CNRS, F-38026 Grenoble Cedex, France*
[f] *Commissariat à l'Energie Atomique, Service de Physique Nucléaire, BP 12, F-91680 Bruyères-le-Châtel, France*
[g] *Centre d'Etudes Nucléaires de Bordeaux Gradignan, F-33175 Gradignan Cedex, France*
[h] *CERN, CH-1211 Geneva 23, Switzerland*
[i] *Centre de Spectrométrie Nucléaire et de Spectrométrie de Masse, IN2P3-CNRS, F-91405 Orsay Cedex, France*
[j] *IN2P3, Paris, France*

Laser spectroscopy measurements have been carried out on very neutron-deficient isotopes of Au, Pt and Ir, produced as daughter elements from a Hg ISOLDE beam. For these transitional region nuclides, the hyperfine structure (HFS) and isotope shift (IS) were measured by Resonance Ionization Spectroscopy (RIS). Magnetic moments μ, spectroscopic quadrupole moments Q_s and changes of the nuclear mean square charge radius $\delta\langle r_c^2\rangle$ along isotopic series have been extracted. For some results, a detailed comparison with theoretical predictions is presented.

1. Introduction

Hyperfine structure (HFS) and isotope shifts (IS) allow direct determination of magnetic moments μ, spectroscopic quadrupole moments Q_s and changes in the mean square charge radius $\delta\langle r_c^2\rangle$ of nuclei. The $\delta\langle r_c^2\rangle$ value is extracted from the isotope shift which is the frequency displacement of the center of gravity of the hyperfine

* Permanent address: Corning S.A., Centre Européen de Recherche de Fontainebleau, F-77210 Avon, France.
** Permanent address: Flerov Laboratory of Nuclear Reaction, JINR, Dubna 141980, Moscow Region, Russia.

spectrum from one isotope to the next. It provides decisive information on the evolution of nuclear deformation along an isotopic series. For odd–even and doubly-odd nuclei, magnetic moments μ are deduced from HFS spectra. Spectroscopic quadrupole moments Q_{s} of nuclear states with spin values higher than $1/2$ are also determined from HFS spectra. These μ and Q_{s} values help to characterize the structure of the states and give the deformation sign for axially symmetric nuclei.

Laser spectroscopy at ISOLDE is an outstanding way of studying nuclear deformation and structure to the limits of stability. Complementing the collinear laser spectroscopy studies long pursued at ISOLDE (Neugart et al., this issue), the COMPLIS experiment concentrates on elements which are not accessible as ISOLDE ion beams. The COMPLIS setup has been designed to perform high-resolution Resonance Ionization Spectroscopy (RIS) on a pulsed secondary atomic beam of daughter nuclides produced by laser desorption. For the first time a coherent study of the transitional nuclei of the refractory elements below Hg has been achieved. This work goes far beyond similar experiments at ISOLDE [1] and ISOCELE [2]. These nuclei have also been investigated extensively by nuclear spectroscopy studies using on-line mass separators [3,5] and heavy-ion reactions [6–12]. Recently, high resolution conversion electron measurements performed at ISOLDE provided important information about ^{183}Pt$^{\mathrm{g,m}}$ [13] and ^{182}Ir, for this work (Roussière et al., this issue).

Some of the COMPLIS results have already been reported in conferences or published [14–25]. After a short description of the experimental procedure and the COMPLIS setup, the effects of the magnetic and electrostatic interactions on the fine levels (hyperfine structure) will be briefly recalled. We will then present and discuss the main results, what we have learnt, and the open questions.

2. Experimental setup and procedure

The neutron-deficient gold, platinum and iridium atoms are obtained by β^+/EC or α-decay of mercury isotopes. The latter are produced, via (p,3pxn) reactions, by bombarding a molten lead target with the 1 GeV staggered proton beam delivered by the PS-Booster [26]. The Hg ions are extracted at 60 kV and mass separated by either the general purpose separator or the high resolution separator. They enter the COMPLIS beam line where they are guided by electrostatic elements and a magnet, are slowed from 60 kV down to 1 kV and implanted into the first atomic layers of a graphite collecting disk (see figure 1). After a delay defined to optimize the amount of Au, Pt or Ir decaying from the collected Hg, the descendant atoms are desorbed using a pulsed, frequency-doubled Nd: YAG laser beam. This produces the pulsed secondary atomic cloud of Au, Pt or Ir. Some microseconds later the desorbed atoms are ionized in a two (for Au) or three (for Pt and Ir) step RIS process (inset, figure 1). The resulting photoions are then accelerated by the 59 kV high voltage of the retardation lens. They are deflected in a symmetrical way relative to that of the incident ions by the magnet. Then, they are guided to a microchannel plate (MCP) detector and mass-identified by their time of flight. For each frequency step, the ion signal is integrated using a digital

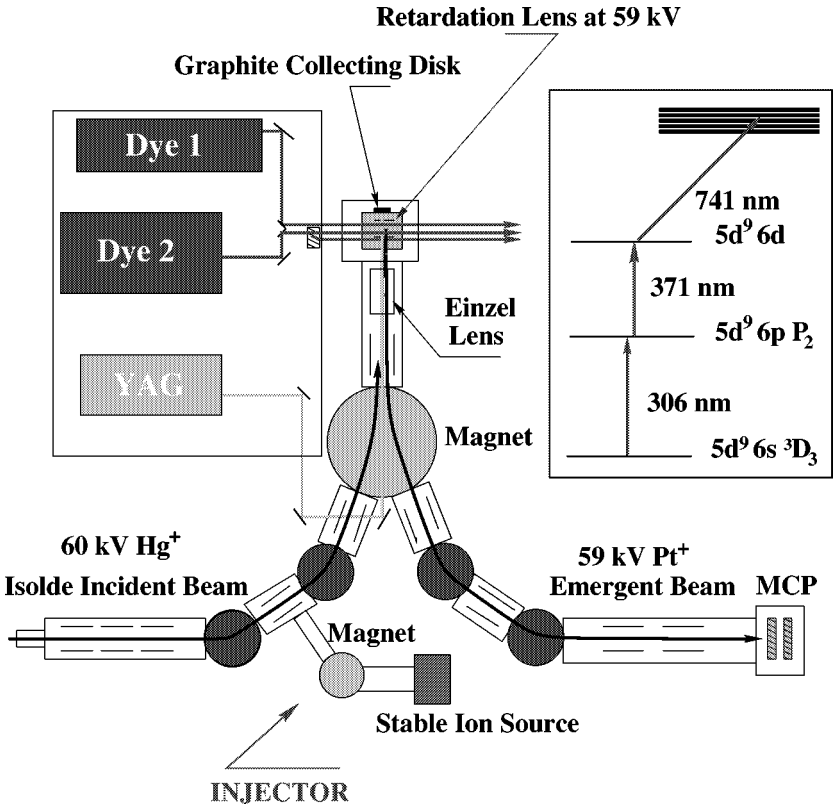

Figure 1. The COMPLIS setup. The insert shows the ionization scheme used for platinum atoms.

oscilloscope and the data are sent into a multitask SUN workstation that also controls the motion of the collecting disk, the firing of the laser and the frequency scan. An injector (an auxiliary ion source coupled to a small mass spectrometer) allows us to send stable ion beams of Au, Pt or Ir into the COMPLIS incident beam line before the experiment, in order to optimize the ionization and desorption efficiencies (see figure 1).

The COMPLIS laser system is shown in figure 2. To obtain a hyperfine spectrum, the first excitation step of the RIS scheme is scanned. To produce the required single-mode pulses, a dye cell pumped by a second frequency-doubled Nd:YAG laser is inserted into the cavity of a commercial cw single mode tunable dye laser (Coherent model 599) [27]. The resulting pulses are further amplified in two additional dye cells. The ionization step is obtained using a Lambdaphysik dye laser pumped by the same Nd:YAG laser. The two laser beams cross at right angles in the interaction region to reduce Doppler linewidth broadening. The time synchronization of the pulses is insured by adjustment of an optical delay line. The cw radiation is analysed by a fixed 10 cm spacing confocal Fabry–Perot interferometer, which provides the frequency-scale.

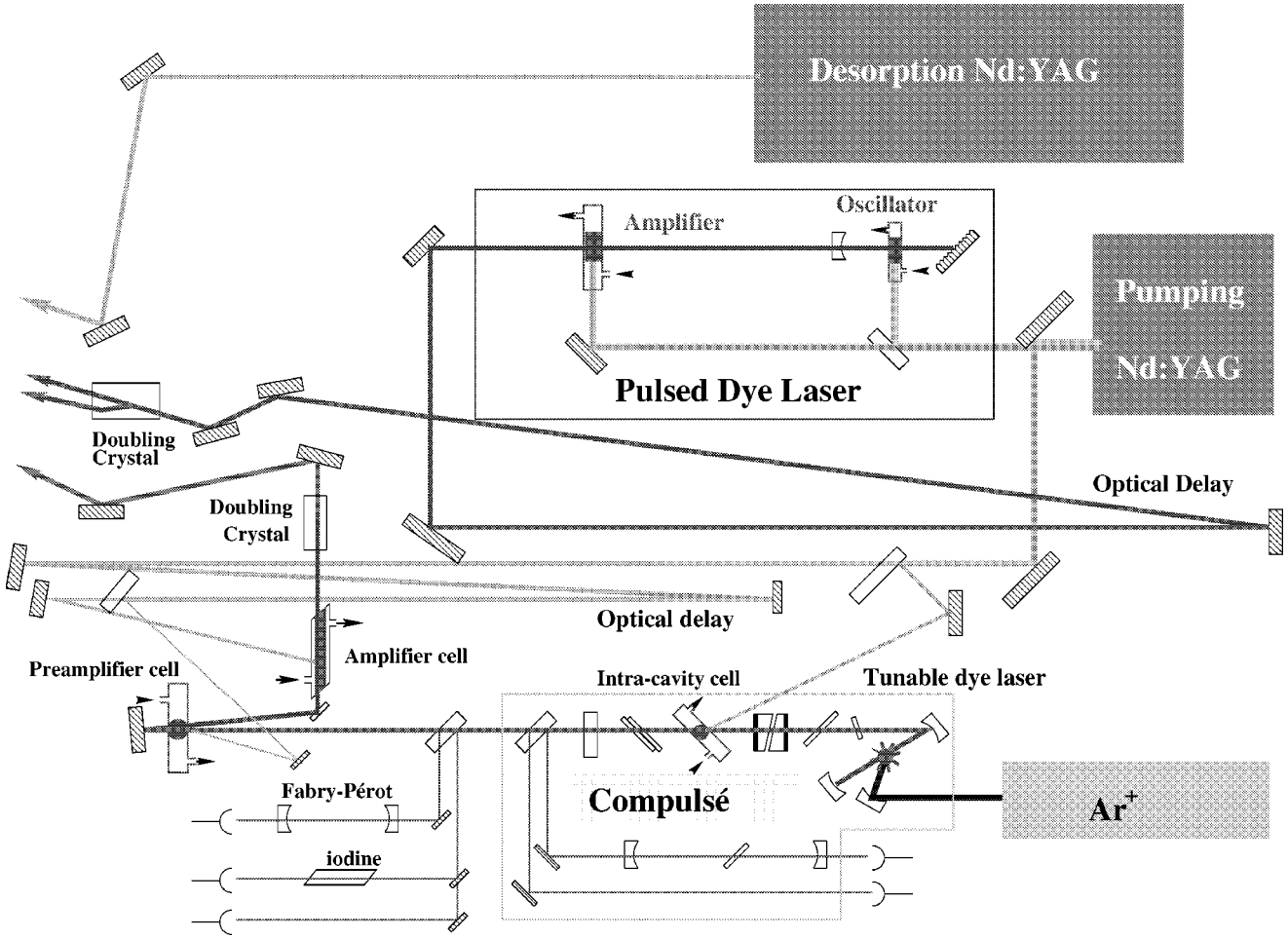

Figure 2. The laser setup as used for platinum in the COMPLIS experiment.

- *For Au atoms*, the first excitation step of the RIS process corresponds to the $5d^{10}\,6s\,^2S_{1/2} \rightarrow 5d^{10}\,6p\,^2P_{3/2}$ optical transition at 243 nm. For this wavelength, single mode laser pulses at 729 nm are frequency tripled using ADP and Urea nonlinear crystals. The ionizing step at 300 nm is obtained by the frequency doubled radiation from the Lambdaphysik dye laser.
- *For Pt atoms*, the first step corresponds to the $5d^9\,6s\,^3D_3 \rightarrow 5d^9\,6p\,^3P_2$ transition at 306.5 nm. The single mode laser pulses are obtained from frequency doubling. For the ionization, the Lambdaphysik dye laser delivers a beam at 742 nm while its frequency doubled radiation at 371 nm induces the second excitation step.
- *For Ir atoms*, the $5d^7\,6s^2\,^4F_{9/2} \rightarrow 5d^7\,6s6p\,^6F_{11/2}$ optical transition at 351.5 nm is used for the first excitation step. The laser pulses are produced by frequency doubling. The Lambdaphysik dye laser delivers radiation at 646 nm for the ionization step. The second excitation step at 323 nm is carried out with the frequency doubled radiation of the 646 nm ionizing beam.

With the COMPLIS setup, good frequency resolution is obtained but at the expense of efficiency; the overall efficiency is typically 10^{-5} for a frequency resolution around 300 MHz. It has been shown that the desorption efficiency depends strongly on the type of graphite used to collect the Hg ions [18].

3. Hyperfine structure and isotope shift

The total energy W_F of a HFS level is given by summing three terms: (i) the energy of the original fine level W_J, (ii) the change in energy due to the level splitting produced by the magnetic interaction between the nuclear magnetic moment μ and the magnetic field $\overline{H}(0)$ that the electrons produce at the nucleus, and (iii) the shift in energy due to the electrostatic interaction between the nuclear quadrupole moment Q_s and the electric field gradient at the nucleus of the orbital electrons $\overline{\varphi}_{JJ}(0)$:

$$W_F = W_J + \frac{AC}{2} + \frac{B\big(3C(C+1) - 4I(I+1)J(J+1)\big)}{8I(2I-1)J(2J-1)}, \tag{1}$$

where I is the nuclear angular momentum, J is the electronic angular momentum, and $\vec{F} = \vec{I} + \vec{J}$ is the total angular momentum of the atom. C is defined as $C = F(F+1) - I(I+1) - J(J+1)$.

The magnetic hyperfine constant A, the electrostatic hyperfine constant B are given by the following expressions:

$$A = \frac{\mu\overline{H}(0)}{I,J}, \tag{2}$$

$$B = eQ_\mathrm{s}\overline{\varphi}_{JJ}(0). \tag{3}$$

In the COMPLIS experiment, the laser beam producing the first excitation step of the RIS process allows the measurement of the resonant lines that correspond to

the electronic transition between different HFS multiplets with $W_F(W_j, A, B, I, J)$ and $W'_F(W'_{J'}, A', B', I, J')$ energies. For atoms with an even–even nucleus only one electronic transition, with an energy $\Delta W = W'_{J'} - W_J$, is observed since no magnetic and electrostatic interactions exist ($\mu = 0,\ Q_\mathrm{s} = 0,\ I = 0$). The centers of gravity of the HFS multiplets remain at the $W'_{J'}$ and W_J energies. Thus, in all cases, the measured isotope shift $\delta\nu$ corresponds to the change of the ΔW energy for neighbouring isotopes. More details can be found in [28–30].

Nuclear moments. We need the $\overline{H}(0)$ and $\overline{\varphi}_{JJ}(0)$ values to extract μ and Q_s from the measured hyperfine constants A and B (see eqs. (2), (3)). But $\overline{H}(0)$ and $\overline{\varphi}_{JJ}(0)$ depend only on Z. They are supposed to be constant along an isotopic series. Thus, they are eliminated if we can use, as a reference, the $A_\mathrm{R},\ \mu_\mathrm{R},\ I_\mathrm{R}$ and $B_\mathrm{R},\ Q_\mathrm{sR}$ values of a stable isotope. The μ and Q_s values are then given by the following relations:

$$\mu = \frac{\mu_\mathrm{R} A I}{A_\mathrm{R} I_\mathrm{R}}, \tag{4}$$

$$Q_\mathrm{s} = \frac{B Q_\mathrm{SR}}{B_\mathrm{R}}. \tag{5}$$

The hyperfine anomaly is due to the fact that the magnetic contribution extends over the entire nuclear volume, which slightly affects $\overline{H}(0)$. Thus, the nucleus cannot be considered as a point nucleus. However, when neglecting this anomaly, expression (4) is usually valid within a few percent. The Q_s calculated using expression (5) has to be corrected by some percent because of the Sternheimer effect. This effect is due to the other s and $\mathrm{p}_{1/2}$ electrons that are inside the nucleus and screen the charge distribution seen by the electron involved in the atomic transition. It can be semi-empirically calculated for a sublevel [31].

Assuming axial symmetry, the intrinsic quadrupole moment Q_0 is given by the expression:

$$Q_0 = Q_\mathrm{s,corr} \frac{(I+1)(2I+3)}{3K^2 - I(I+1)}, \tag{6}$$

where K is the projection of I on the nuclear symmetry axis and $Q_\mathrm{s,corr}$ the Q_s value corrected, if necessary, for the Sternheimer shielding factor (see below). The β deformation parameter is then calculated using the relation

$$Q_0 = \frac{3}{\sqrt{5\pi}} Z R_0^2 \beta \left(1 + \frac{2}{7}\sqrt{\frac{5}{\pi}}\beta\right) \tag{7}$$

with $R_0 = 1.2A^{1/3}$.

Change in the mean square charge radius. The measured IS $\delta\nu^{A,A'}$ between the isotopes of mass A and A' consists of a mass shift and a field shift [32]. The mass

shift, which is small for heavy elements, can be estimated as described in [33]. The field shift can be expressed as [34]

$$\delta\nu_{\mathrm{FS}}^{A,A'} = kF\delta\langle r^2\rangle, \tag{8}$$

where F is the electronic factor of the atomic transition. F depends on the variation of the electronic probability density at the nucleus during the transition. It is usually obtained by MCDF calculations or by a King plot [35]. k is calculated using the Seltzer coefficient [32] as described in [34].

The mean-square deformation parameter change $\delta\langle\beta^2\rangle^{A,A'}$ can be extracted via [29]

$$\delta\langle r^2\rangle^{A,A'} = \delta\langle r^2\rangle_{\mathrm{sph}}^{A,A'} + \frac{5}{4\pi}\langle r^2\rangle_{\mathrm{sph}}\delta\langle\beta^2\rangle^{A,A'}, \tag{9}$$

where $\delta\langle r^2\rangle_{\mathrm{sph}}^{A,A'}$ and $\langle r^2\rangle_{\mathrm{sph}}$ are calculated using the droplet model [36].

4. Experimental results and discussion

For Au isotopes, HFS spectra were recorded for the ^{188,190,191,193,195,197}Au and ^{184}Au^{g+m} atoms. The measurement of ^{184}Au^{g+m} was especially challenging because the half-lives of both states are rather short: $T_{1/2m} \sim 45$ s and $T_{1/2g} \sim 20$ s [37,38] or $T_{1/2m} = 28$ s and $T_{1/2g} = 12$ s [39]. For each state, the relative positions of the six resonant lines have allowed the extraction of the magnetic hyperfine constants of the two atomic levels, A and A', the electrostatic hyperfine constant of the final state, B', and the isomeric shift. Furthermore, the IS relative to the stable mass ^{197}Au has been determined for all of the recorded HFS spectra. The Q_{s} and μ values have been calculated using ^{197}Au as a reference. Indeed, for this nucleus, Q_{s} has been measured from a muonic X-ray experiment [40] as well as B' [41]. On the other hand, A and μ have been precisely measured [42]. However, ^{197}Au exhibits a strong hyperfine anomaly so the relation (4) cannot be used. Ekström et al. [43] have shown that, neglecting the hyperfine anomaly for the other gold isotopes, the μ values can be determined using the following relation [43]:

$$\mu = (AI/29.005)\mu_{\mathrm{N}}.$$

The hyperfine structure anomaly uncertainty is less than 10% [43]. The $\delta\langle r^2\rangle$ value has been obtained using the electronic factor F_{243} given by a relativistic multiconfiguration Dirac–Fock (MCDF) calculation [44]:

$$\mathrm{F}_{243} = -42.73\ \mathrm{GHz/fm}^2.$$

The deformation of ^{197}Au ($\beta = 0.113$) used as a reference is taken from the calculations of Möller and Nix [45].

For Pt isotopes, the HFS spectra of ^{183}Pt^{g} and ^{185}Pt^{g+m} atoms were more precisely measured than in previous experiments [1,2] whereas the HFS spectra of

$^{178-182}$Pt and ^{183}Pt^{m} were recorded for the first time. The measurement of the very exotic $^{178-181}$Pt could be performed because they are obtained not by two successive β^+/EC decays of $^{178-181}$Hg but by the α-decay of $^{182-185}$Hg atoms that are produced with much higher yields than $^{178-181}$Hg. For the odd isotopes with a nuclear spin value $I = 1/2$, only the magnetic hyperfine constants of the two atomic levels, A and A', could be deduced from the hyperfine spectrum. For ^{183}Pt^{m} and ^{185}Pt^{g} in addition to the A and A' constants, it was possible to extract the electrostatic hyperfine constants of the two atomic levels, B and B'. For all recorded HFS spectra the IS were measured relative to the stable mass ^{194}Pt. The μ values have been calculated from the precisely known μ and A values of the ^{195}Pt ground state [46,47]. The errors on μ include the hyperfine structure anomaly uncertainties [1,25]. No Q_s value of ^{195}Pt could be measured since its angular momentum is $1/2$. So, we used the $\overline{\varphi}_{JJ}(0)$ calculated by Hilberath et al. [1] to deduce the Q_s values from the measured B values. Then, the Q_s values have been corrected for the Sternheimer shielding factor that is estimated to be $R = -0.1$ in the 5d shell [31]:

$$Q_{s,corr} = \frac{Q_s}{1 - R}.$$

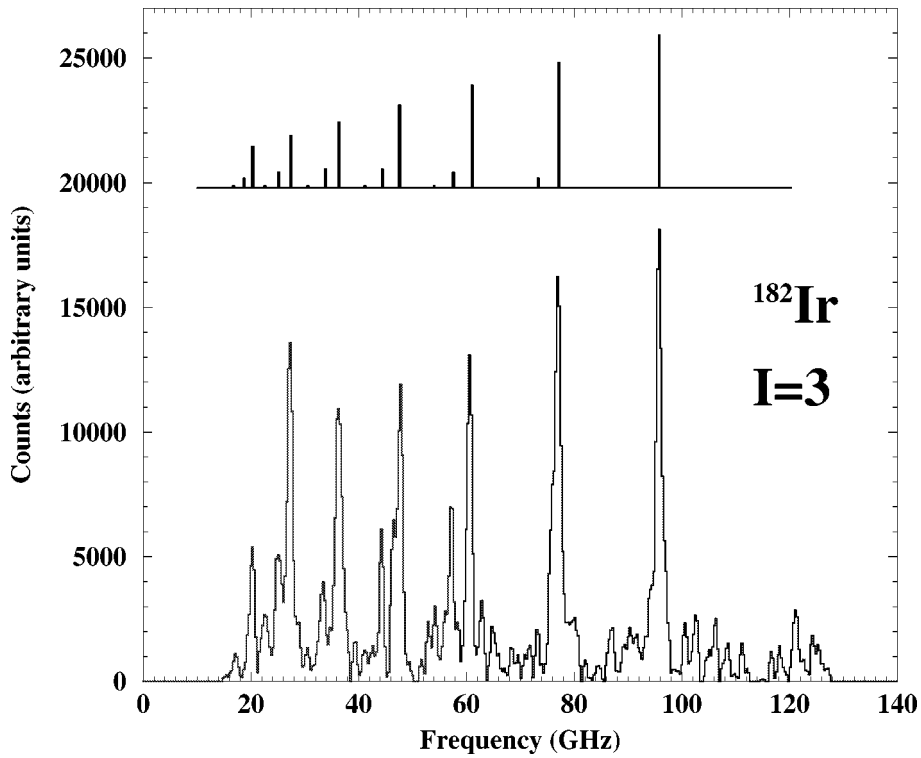

Figure 3. Hyperfine spectrum of ^{182}Ir. The theoretical spectrum (top) has been calculated with the hyperfine constants A, A', B and B' extracted from the experimental spectrum (bottom).

The $\delta\langle r^2\rangle$ values have been determined using the F_{306} value derived from a King plot [25]

$$F_{306} = -18.5(10)\ \mathrm{GHz/fm^2}.$$

The deformation of ^{194}Pt ($\beta = 0.1434(26)$) deduced from a B(E2) value [48] is used as a reference.

For Ir isotopes, the HFS spectra of $^{182-189}$Ir and ^{186}Ir^{m} were recorded for the first time. The spectra of the stable masses ^{191,193}Ir have also been measured. For all these masses, the hyperfine constants of the two atomic levels A, A' and B, B' could be deduced. For the light isotopes the HFS spectra are extremely wide; for example, the ^{186}Ir spectrum spans about 100 GHz. The IS have been determined relative to ^{191}Ir. The ^{182}Ir HFS spectrum, over 80 GHz wide, is shown as an example in figure 3. The μ and Q_s values have been determined using the known A, μ and B, Q_s values of the ^{191}Ir ground state [49–51] as in [52].

The preliminary $\delta\langle r^2\rangle$ results have been estimated [52] using the F factor deduced from the λ value measured by Sawatzky and Winkler [53], but MCDF calculations are in progress.

The μ and Q_s values of the Au and Pt isotopes measured by COMPLIS are reported in table 1. The intrinsic quadrupole moments Q_0 are calculated assuming an axial symmetry for the nucleus and using the I and K values given in column 3 of table 1 (K is the projection, on the symmetry axis, of the angular momentum I). The nuclear deformation parameter β is then deduced from the Q_0 value. The $\langle\beta^2\rangle^{1/2}$ is the deformation parameter value extracted from the IS data [20–23,25]. An important feature is evident in table 1: the β value deduced from the Q_0 value is in rather good agreement with the $\langle\beta^2\rangle^{1/2}$ value provided by the IS data, which shows that the axial symmetry we assumed to calculate Q_0 is fully justified, at least for ^{184}Au and ^{183,185}Pt. The cases of ^{191,193,195}Au and ^{187,189}Pt with $I = 3/2$ are more complicated [1,54] and will be discussed below. In the doubly-odd nucleus ^{184}Au, the results imply that the $I = 2^+$ isomeric and $I = 5^+$ ground states very likely correspond to the $\pi 3/2[5\,3\,2]\otimes\nu 1/2[5\,2\,1]$ and $\pi 3/2[5\,3\,2]\otimes\nu 7/2[5\,1\,4]$ structures, respectively. For the odd nuclei, the theoretical magnetic moments μ_{cal} are calculated using the axial-rotor+ one-quasiparticle (AR + 1QP) coupling model [55,56] for $g_s = g_{s\,free}$ (0.6 $g_{s\,free}$) and $g_R = Z/A$ [23]. For ^{184}Au the μ_{cal} values have been estimated using the formula [57]:

$$\mu_{cal} = \frac{K(g_{Kp}K_p + g_{Kn}K_n + g_R)}{I(I+1)},$$

where g_{Kp} and g_{Kn} are deduced from the μ values calculated in the neighbouring odd isotopes. The satisfactory agreement between μ and μ_{cal} confirms the structures previously proposed for ^{184}Au and ^{179,181,183,185}Pt isomeric and ground states [3,7,13, 58–62].

The measured μ values of ^{184}Au^{g,m}, ^{185}Pt^{g} and ^{183}Pt^{m} confirm the single-particle states involved and thus determine their I and K values. These I and K lead to positive

Table 1
Nuclear moments and deformation parameter for Au and Pt isotopes.

Nucleus mass	μ (μ_N)	State[1] $I\ K\ [Nn_z\Lambda]$	μ_{cal} $g_{sfree}(0.6g_{sfree})$	Q_s (b)	Q_0[2] (b)	β from Q_0	$\langle\beta^2\rangle^{1/2}$ from IS
Au							
195	+0.150(7)	3/2 3/2 [4 0 2]		+0.62(6)	+3.10(30)	+0.103(10)	0.123(1)
193	+0.145(8)	3/2 3/2 [4 0 2]	−0.12(+0.52)	+0.69(8)	+3.45(40)	+0.115(13)	0.132(1)
191	+0.137(3)	3/2 3/2 [4 0 2]		+0.76(3)	+3.80(15)	+0.127(5)	0.140(1)
184g	+2.07(2)	π3/2 [5 3 2]⊕ ν7/2 [5 1 4] $I = K = 5$	+2.3(+2.2)	+4.65(26)	+8.06(45)	+0.264(14)	0.255(3)
184m	+1.44(2)	π3/2 [5 3 2]⊕ ν1/2 [5 2 1] $I = K = 2$	+1.2(+1.4)	+1.90(16)	+6.65(56)	+0.221(17)	0.249(3)
Pt							
189	−0.422(7)	3/2 3/2 [5 3 2]	+0.24(+0.22)	−0.956(84)	−4.35(38)	−0.165(15)	0.165(3)
		3/2 1/2 [5 1 0][3]	−0.0013(+0.11)		+4.35(38)	+0.165(15)	
187	−0.399(8)	3/2 3/2 [5 3 2]		−1.08(6)	−4.90(25)	−0.189(8)	0.191(3)
		3/2 1/2 [5 1 0][4]	−0.21(−0.0014)		+4.90(25)	+0.189(8)	
185g	−0.723(11)	9/2 9/2 [6 2 4]	−1.46(−0.86)	+4.10(19)	+6.84(31)	+0.229(10)	0.231(3)
185m	+0.503(5)	1/2 1/2 [5 2 1]	+0.63(+0.37)				0.207(3)
183g	+0.502(5)	1/2 1/2 [5 2 1]	+0.63(+0.37)				0.227(3)
183m	+0.782(14)	7/2 7/2 [5 1 4]	+1.46(+0.99)	+3.71(30)	+7.22(58)	+0.242(18)	0.246(3)
181	+0.484(21)	1/2 1/2 [5 2 1]	+0.63(+0.38)				0.239(4)
179	+0.431(32)	1/2 1/2 [5 2 1]	+0.64(+0.38)				0.243(5)

[1] Main component of the wave function.
[2] For Pt, Q_0 values have been calculated from Q_s values corrected for the Sternheimer shielding factor.
[3] The component on 1/2 [5 1 0] is only 52%.
[4] The component on 1/2 [5 1 0] is 65%.

Q_0 and β values. Moreover, the deformations deduced from Q_0 are consistent with those extracted from $\delta\langle r^2\rangle$ values. Therefore, we can conclude that ^{184}Au^{g+m}, ^{185}Pt^{g} and ^{183}Pt^{m} most probably have a prolate shape.

Our ^{191,193,195}Au results confirm those previously reported [54,63]. We can note that the measured μ values are close to those known for the 3/2 [4 0 2] state of ^{189,191,193}Ir (0.13, +0.1507 and +0.1637 μ_N, respectively) [64]. Moreover, this 3/2 [4 0 2] state is predicted to be the ground state of ^{191,193,195}Au in our AR + 1QP calculation for a $\beta = \langle\beta^2\rangle^{1/2}$ prolate deformation and its μ_{cal} agrees with the measured value. Thus, all the results are compatible with ^{191,193,195}Au prolate-shaped nuclei as already mentioned in [63]. However, we have to note that a study performed on another type of data, namely, cross sections, led Delaroche [65] to infer an oblate shape for ^{197}Au of which the ground state has the same structure as ^{191,193,195}Au.

As for ^{187,189}Pt, the results correspond either to a $I = K = 3/2$ state for an oblate shape or to a $I = 3/2$ $K = 1/2$ state for a prolate shape. In the case of an oblate shape, no $I = K = 3/2$ state having a negative μ value is predicted lying below

1.5 MeV, the $3/2\ 3/2$ [5 3 2] state being the lowest one. On the other hand, in the case of a prolate shape, the $3/2\ 1/2$ [5 1 0] state lying below 130 keV has a negative μ value. Moreover, we note that the measured μ values are similar to that of the $3/2\ 1/2$ [5 1 0] state of ^{189}Os ($-0.32\ \mu_{\mathrm{N}}$) [64]. It is worth noting that the μ_{cal} value varies rather quickly against the β value because of the quick change of the admixture of the $3/2\ 1/2$ [5 1 0] and $3/2\ 3/2$ [5 1 2] states, under the Coriolis force. Thus, the μ value observed is compatible with a prolate shape for ^{187,189}Pt. Nevertheless, given that Q_0 has been calculated assuming a pure $K = 1/2$ state, one must wonder whether the wave functions are well represented or whether the axial symmetry assumed is actually justified.

Finally, the results contain some clues that suggest a weakly deformed prolate shape for the heavy odd-A Au and Pt isotopes. This raises questions about the shape of the $3/2^-$ ^{187,189,191,193}Hg ground states that also have negative μ values still unexplained [64]. Indeed, the ^{187,189,191}Pt and ^{187,189,191,193}Hg $3/2^-$ ground states have similarly small deformations and, whatever their nuclear shape may be, the same neutron states are expected to be close to the Fermi level. Therefore, the negative μ values of the $3/2^-$ Hg ground states can very likely be explained only if this $3/2^-$ state corresponds mainly to the prolate $3/2\ 1/2$ [5 1 0] neutron state as discussed above for the ^{187,189}Pt ground states. This has to be confirmed by more calculations.

For the Ir isotopes the preliminary μ and Q_{s} values we obtained for $^{184-189}$Ir confirm the values previously determined by different methods [64,66].

In figure 4 are shown the $\delta\langle r_{\mathrm{c}}^2\rangle$ values determined by COMPLIS for Au, Pt and Ir isotopes together with those previously measured for Au [67–69] and Pt [1,2]. A progressive decrease of the change in the mean square charge radius as the neutron number diminishes, corresponds to an increase in deformation (see eq. (9)). So, for the even Pt nuclei, we can see in figure 4 that the deformation increases from $A = 188$ to $A = 180$ and starts to decrease for $A = 178$. Thus, the maximum deformation is found for $N = 102$. Furthermore, in addition to a strong inverted odd–even staggering that appears around the neutron mid-shell in the Pt isotopes, a deformation change is indicated between isomeric and ground states of the ^{184}Au, ^{183,185}Pt and ^{186}Ir nuclei. These results show that the nuclear deformation is highly influenced by the coupling of one or two single quasiparticles to the core, illustrating the softness of these exotic nuclei. In the case of the Pt isotopes, the comparison of the determined $\delta\langle r_{\mathrm{c}}^2\rangle$ values with those predicted in the framework of microscopic Hartree–Fock–Bogoliubov (HFB) calculations using the Gogny force suggests that the odd–even staggering observed around $N = 104$ is due to shape changes: the even Pt isotopes have a triaxial shape with an asymmetry parameter γ around 15°, and the odd Pt nuclei a prolate shape as already suggested by the nuclear moment values [25].

The energy position of the $1/2^-$ and $7/2^-$ neutron states is inverted in ^{184}Au relative to their position in ^{183}Pt. The deformation changes measured for ^{183}Pt$^{\mathrm{g,m}}$ and ^{184}Au$^{\mathrm{g,m}}$ allow us to explain qualitatively the state inversion observed in ^{184}Au [20, 21,23,70]. Another important result concerns the $3/2$ [5 3 2] proton state involved in the structure of ^{184}Au$^{\mathrm{g,m}}$. Indeed, this orbital is originating from the $\mathrm{h}_{9/2}$ subshell. In

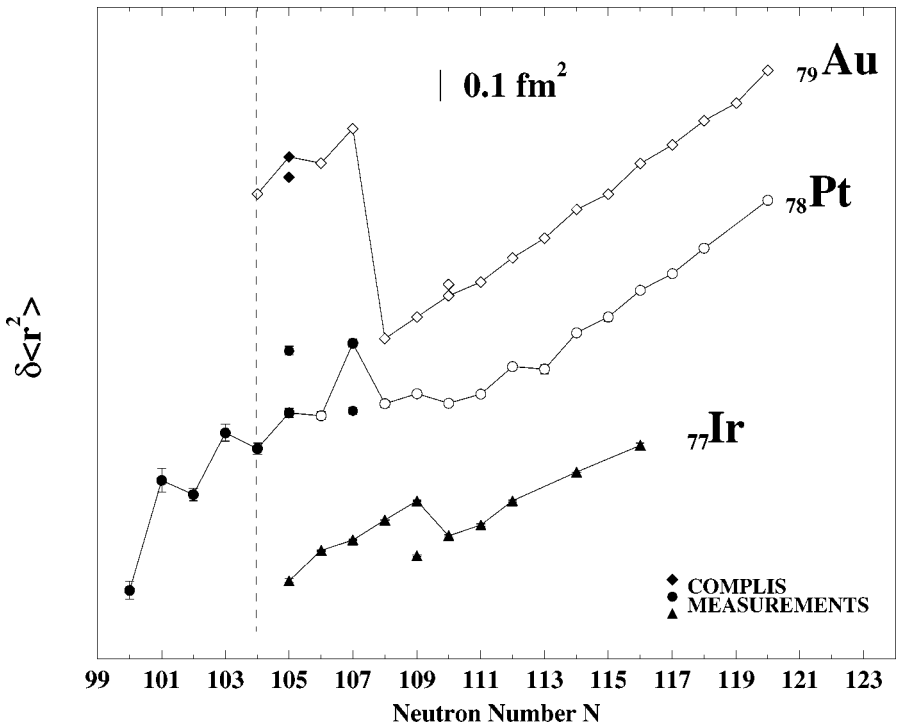

Figure 4. $\delta\langle r_c^2\rangle$ values for ^{184}Au^{g,m}, $^{178-185}$Pt, ^{183,185}Pt^{m} determined in this work and those taken from [67–69] and [1,2] for the other Au and Pt isotopes. The preliminary values displayed for $^{182-189,191,193}$Ir have been estimated using the F-factor deduced from a measured λ value [53]. The values not connected by lines correspond to isomeric states.

^{183,185}Au, the $h_{9/2}$ proton is decoupled from the core under the Coriolis force [71–73]. It becomes the strongly coupled $3/2$ [5 3 2] proton state in the doubly odd ^{184}Au nucleus [20]. The $h_{9/2}$ proton is involved in the ground state structure of most of the Ir isotopes. So, to get a better understanding of the proton coupling change phenomenon we are performing theoretical calculations for the Ir isotopes. Thus, the comparison between results on Au and Ir isotopes will allow us to study the influence of the Fermi level position on the proton coupling mode, as a function of the proton number and deformation.

In the present work we have shown that measurements of HFS, especially as Q_s can be measured, provide decisive information on nuclear shapes and wave functions of isomeric and ground states. From the $\delta\langle r^2\rangle$ curves shown in figure 4, one can see that the odd-proton Ir and Au isotopes have a similar behavior. A sudden deformation increase is observed between $A = 187$ and $A = 186$ that can be associated with the change of the proton state that is the $3/2^+$ [4 0 2] or $1/2^+$ [4 0 0] state for $A \geqslant 186$ and becomes the $5/2\ 1/2^-$ [5 4 1] or $3/2\ 3/2^-$ [5 3 2] intruder state arising from the $h_{9/2}$ subshell for $A \leqslant 186$ [52]. We have to note that the coupling of a neutron to the single proton has little or no influence on the nuclear deformation of both the Au

and Ir isotopes. On the other hand, for the even-proton Pt isotopes with $A < 186$, the coupling of a neutron to an even–even core highly influences the nuclear deformation, whatever the involved neutron state may be (figure 4). This behavior is similar to that already observed for the coupling of the $1/2^-$ [5 2 1] neutron state, in the Hg isotopes [74]. Moreover, for this $1/2^-$ [5 2 1] neutron state, the odd–even staggering increases as A decreases for both the Hg and Pt isotopes [70,74].

Nevertheless, in general, the nuclear deformation changes observed below $A = 186$ are less and less pronounced as the proton number drops below $Z = 82$. This rather high instability in deformation could be due to the presence of the neutron midshell located very far from the β stability valley for these elements. The beginning of a deformation instability has also been observed around the neutron midshell $N = 66$ for the Ba and Cs isotopes located far from stability [15].

In the future we plan to extend such laser spectroscopy studies to the Sn region around $N = 82$. The goal of these experiments on neutron-rich nuclei will be to study the effect of crossing the neutron magic number $N = 82$, on the $\delta\langle r_c^2\rangle$ values.

References

[1] T. Hilberath et al., Z. Phys. A 342 (1992) 1.
[2] H.T. Duong et al., Phys. Lett. B 217 (1989) 401.
[3] F. Ibrahim et al., Z. Phys. A 350 (1994) 9.
[4] D. Rupnik et al., Phys. Rev. C 58 (1998) 771.
[5] J. Sauvage et al., Nuclear Phys. A 592 (1995) 221.
[6] G. Hebbinghaus et al., Nuclear Phys. A 514 (1990) 225.
[7] M.J.A. De Voigt et al., Nuclear Phys. A 507 (1990) 447.
[8] A.J. Kreiner et al., Phys. Rev. C 42 (1990) 878.
[9] G.D. Dracoulis et al., Phys. Rev. C 44 (1991) R1216.
[10] V.P. Janzen et al., Phys. Rev. C 45 (1992) 613.
[11] D. Seweryniak et al., Phys. Rev. C 58 (1998) 2710.
[12] B. Cederwall et al., JYFL Annual Report (1997) p. 31.
[13] B. Roussière et al., Nuclear Phys. A 643 (1998) 331.
[14] N. Boos et al., in: *Workshop on Nuclear Shapes and Nuclear Structure at Low Excitation Energies*, Cargèse (1991).
[15] J. Sauvage, in: *Proc. of the 6th Franco-Japanese Coll. on Nuclear Structure and Interdisciplinary Topics*, Saint-Malo (1992), eds. N. Alamanos, S. Fortier and F. Dykstra (Commissariat à l'Energie Atomique, 1993) p. 300.
[16] F. Le Blanc et al., in: *Proc. of the 8th Internat. Symp. on Capture Gamma-Ray Spectroscopy and Related Topics*, Fribourg (1993), ed. J. Kern (World Scientific, Singapore, 1994) p. 1001.
[17] F. Le Blanc et al., in: *Proc. of the Internat. Conf. on Exotic Nuclei and Atomic Masses, ENAM '95*, Arles (1995), eds. M. De Saint-Simon and O. Sorlin (Frontières, 1995) p. 141.
[18] J. Pinard et al., in: *Proc. of the 3rd Internat. Workshop on Hyperfine Structure and Nuclear Moments of Exotic Nuclei by Laser Spectroscopy*, Poznan (1997) (Joint Institute for Nuclear Research, Dubna, 1998) p. 30.
[19] B. Roussière et al., in: *Proc. of Internat. Symp. on Exotic Nuclear Shapes*, Debrecen (1997), eds. Z.S. Dombradi, Z. Gacsi and A. Krasznahorkay, Akadémiai Kiado, Budapest, Heavy Ion Physics 7 (1998) 97.
[20] F. Le Blanc et al., Phys. Rev. Lett. 79 (1997) 2213.

[21] J. Sauvage et al., in: *Proc. of the 2nd Internat. Conf. on Exotic Nuclei and Atomic Masses, ENAM '98*, Bellaire (1998);
B.M. Sherill, D.J. Morrissey and C.N. Davids, in: AIP Conf. Proc. 455 (1998) p. 585.
[22] F. Le Blanc et al., in: *Proc. of the 2nd Internat. Conf. on Exotic Nuclei and Atomic Masses, ENAM '98*, Bellaire (1998);
B.M. Sherill, D.J. Morrissey and C.N. Davids, in: AIP Conf. Proc. 455 (1998) p. 78.
[23] J. Sauvage et al., in: *Proc. of Internat. Conf. on Nuclear Phys. Close to the Barrier*, Warsaw (1998), Acta Physica Polonica B 30 (1999) 1393.
[24] J.E. Crawford et al., in: *Proc. of Resonance Ionization Spectroscopy, RIS '98*, Manchester (1998).
[25] F. Le Blanc et al., Phys. Rev. C 60 (1999) 054310-1.
[26] J. Lettry et al., Nucl. Instrum. Methods B 126 (1997) 170.
[27] J. Pinard and S. Liberman, Opt. Commun. 20 (1977) 344.
[28] H. Kopferman, ed., *Nuclear Moments* (Academic Press, New York, 1958).
[29] E.W. Otten, in: *Treatise on Heavy-Ion Science*, Vol. 8, ed. D.A. Bromley (Plenum, New York, 1989) p. 17.
[30] J. Billowes and P. Campbell, J. Phys. G 21 (1995) 707.
[31] W. Childs and K. Cheng, Phys. Rev. A 30 (1984) 667.
[32] E.C. Seltzer, Phys. Rev. 188 (1969) 1916.
[33] K. Heilig and A. Steudel, At. Data Nucl. Data Tables 14 (1974) 613.
[34] G. Torbhom et al., Phys. Rev. A 31 (1985) 2038.
[35] W.H. King et al., Z. Phys. 265 (1973) 207.
[36] W.D. Myers and K.H. Schmidt, Nuclear Phys. A 410 (1983) 61.
[37] I. Romanski et al., Hyp. Interact. 75 (1992) 457.
[38] K. Zaerpoor et al., Phys. Rev. C 55 (1997) 2697.
[39] A. Knipper, private communication.
[40] R.J. Powers et al., Nuclear. Phys. A 230 (1974) 413.
[41] G. Goldmann, C. Hahn and J. Ney, Z. Phys. 225 (1969) 1.
[42] H. Dahmen and S. Penselin, Z. Phys. 200 (1967) 456.
[43] C. Ekström et al., Nuclear Phys. A 348 (1980) 25.
[44] A. Rosen, B. Fricke and G. Torbohm, Z. Phys. A 316 (1984) 157.
[45] P. Möller and J.R. Nix, At. Data Nucl. Data Tables 26 (1981) 165.
[46] S. Büttgenbach et al., Z. Phys. A 317 (1984) 237.
[47] P. Raghavan, At. Data Nucl. Data Tables 42 (1989) 189.
[48] S. Raman et al., At. Data Nucl. Data Tables 42 (1989) 1.
[49] S. Büttgenbach et al., Z. Phys. A 286 (1978) 333.
[50] K.H. Burger et al., Phys. Lett. B 140 (1984) 17.
[51] Y. Tanaka et al., Phys. Rev. C 29 (1984) 1830.
[52] D. Verney et al., in: *Internat. Conf. on Experimental Nuclear Physics in Europe Facing the Next Millennium*, Sevilla (1999), AIP Conf. Proc. 495 (1999) p. 117.
[53] G. Sawatsky and R. Winkler, Z. Phys. D 14 (1989) 9.
[54] G. Passler et al., Nuclear Phys. A 580 (1994) 173.
[55] M. Meyer et al., Nuclear Phys. A 316 (1979) 93.
[56] J. Libert et al., Phys. Rev. C 25 (1982) 586.
[57] C. Ekström et al., Phys. Scripta 14 (1976) 199.
[58] B. Roussière et al., Nuclear Phys. A 438 (1985) 93.
[59] S. Pilotte at al., Phys. Rev. Lett. 40 (1989) 610.
[60] J. Nyberg et al., Nuclear Phys. A 511 (1990) 92.
[61] J. Sauvage et al., Nuclear Phys. A 540 (1992) 83.
[62] E. Hagberg et al., Nuclear Phys. A 318 (1979) 29.
[63] B. Hinfurtner et al., Nuclear Phys. A 562 (1993) 205.

[64] R.B. Firestone, *8th Table of Isotopes*, Vol. II, ed. V.S. Shirley (Wiley Interscience, New York, 1996).
[65] J.P. Delaroche, in: *Proc. of Internat. Conf. on Neutron Physics and Nuclear Data*, Harwell (1978) (OECD Nuclear Energy Agency, 1978) p. 366.
[66] G. Seewald et al., Phys. Rev. Lett. 77 (1996) 5016.
[67] W. Wallmeroth et al., Nuclear Phys. A 493 (1989) 224.
[68] G. Savard et al., Nuclear Phys. A 512 (1990) 241.
[69] U. Krönert et al., Z. Phys. A 331 (1988) 521.
[70] B. Roussière et al., in: *Proc. of the 48th Meeting on Nuclear Spectroscopy and Nuclear Structure*, Moscow (1998).
[71] C. Bourgeois et al., Nuclear Phys. A 386 (1982) 308.
[72] M.I. Macias-Marques et al., Nuclear Phys. A 427 (1984) 205.
[73] K. Heyde et al., Phys. Rep. 102 (1983) 291.
[74] G. Ulm et al., Z. Phys. A 325 (1986) 247.